Oriented Attachment-Based Assembly of Dendritic Silver Nanostructures at Room Temperature

Lehui Lu,[†] Atsuko Kobayashi,[‡] Yasuo Kikkawa,[†] Keiko Tawa,[‡] and Yukihiro Ozaki*[,†]

Department of Chemistry, School of Science and Technology, Kwansei Gakuin University, Sanda, Hyogo 669-1337, Japan, and National Institute of Advanced Industrial Science and Technology (AIST), Ikeda, Osaka 563-8577, Japan

Received: June 26, 2006; In Final Form: September 15, 2006

How particles aggregate into an interesting dendritic structure has been the object of research for many years because of its importance in understanding physical processes involved and in designing novel materials. In this work, we for the first time describe an oriented attachment-based assembly mechanism for formation of different types of dendritic silver nanostructures at room temperature. It is found that the concentration of both $AgNO_3$ and *p*-aminoazobenzene (PA) molecules has a significant effect on the formation and growth of these novel nanostructures. Characterization by transmission electron microscopy (TEM) clearly shows that the dendritic silver nanostructures can be obtained through the preferential oriented growth along a crystallographically special direction. Interestingly, we observe that the oriented attachment at room temperature can also take place between relatively large single-crystalline silver particles with a diameter range from 20 to 60 nm, which may provide a new possibility for the design of novel metal nanostructures by using large metal nanoparticles as building blocks at room temperature. Moreover, a surface-enhanced Raman scattering (SERS) technique is used to investigate the role of PA molecules during the growth of the dendritic silver nanostructures.

Introduction

Hierarchical assembly of solution-based nanocrystals as building blocks are of great interest because of their potential in controlling morphologies of nanostructures and, hence, their properties.[1−9] Recently, the hierarchical assembly technique has been used widely to prepare nanorods,[2,3] nanowires,[4,5] nanorings,[6] dendrites,[9a] and so forth. Among these nanomaterials, the dendritic supramolecular nanostructures are particularly attractive due to their promising applications in catalyst, sensors, optical and electronic systems, and fluorescence-enhancement materials.[9a,10−12] It is generally accepted that the dendrites form through the hierarchical assembly under nonequilibrium growth conditions, and thus they can provide a natural framework for the investigations of disordered systems. A good understanding of the process and parameters controlling the dendrites formation under nonequilibrium conditions is crucial for achieving the design of novel dendritic nanostructures with desired properties. However, despite a large number of reports on the preparation and theoretical studies of the dendritic nanostructures,[9a,10−12] it has still been a significant challenge to discover common mechanisms underlying their formation such as nucleation and growth.

Nanostructure formation in a solution typically involves the fast nucleation of primary particles and the subsequent growth by two mechanisms: Ostwald ripening and aggregation.[13,14] Ostwald ripening refers to the processes where larger particles grow at the expense of smaller ones, and it is generally believed to be a dominant path for crystal growth. However, recent studies on nanocrystal growth have indicated that such a model does not provide a reasonable explanation in many systems including the semiconductor nanorods, nanowires, and nanorings.[2−6] A very different aggregation-based growth model has recently been proposed by Banfield et al. to rationalize their interesting observation in some natural minerals such as natural iron oxyhydroxide.[15] They found that the adjacent 2- to 3- nm particles can spontaneously aggregate and further grow into bulk crystals in a way that they call "oriented attachment". Perfect single crystals are formed if the adjacent nanoparticles adopt parallel crystallographic orientation, while slight misorientation between them leads to the formation of dislocations. In addition to the natural minerals, the oriented aggregation mechanism has also been observed to play a key role in the preparation of several kinds of nanomaterials including TiO_2,[16] ZnO,[2] SnO_2,[17] Ag,[5] PbSe,[6] and so forth. Nevertheless, we are not aware of a publication on the formation of dendritic silver nanostructures based on the oriented attachment mechanism.

In this work, we demonstrate an oriented attachment-based assembly mechanism for the formation of dendritic silver nanostructures. High-resolution transmission electron microscopy (HRTEM) characterizations of such nanostructures clearly reveal that oriented attachment is a dominant process during the formation and growth of dendritic silver nanostructure. We also investigate the role of *p*-aminoazobenzene molecules during the oriented aggregation by the SERS technique.

Experimental Methods

Materials. *p*-Aminoazobenzene (PA), silver nitrate, ethanol, and rhodamine 6G (R6G) were purchased from Wako Pure Chemical Industries, Ltd. Sodium borohydride was obtained from SIGMA-Aldrich, Inc. All reagents were used as received.

* Author to whom correspondence should be addressed. Tel: +81-79-565-8349. Fax: +81-79-565-9077. E-mail: ozaki@kwansei.ac.jp.
[†] Kwansei Gakuin University.
[‡] National Institute of Advanced Industrial Science and Technology (AIST).

10.1021/jp063978c CCC: $33.50
Published on Web 10/20/2006

Synthesis of Dendritic Silver Nanostructures. In a typical experiment, a solution of PA molecules in ethanol (5 mL, 2 mM) was mixed with an aqueous solution of silver nitrate (20 mL, 3.7 mM). No color change was observed during this procedure. After 5 min, a freshly prepared aqueous solution of sodium borohydride (2 mL, 20 mM) was added to the above mixture under vigorously stirring at room temperature (sample 1: experimental condition 1). The color of the mixture obviously changed from initial light yellow to darker yellow-green after one second, to darker green after 2 h, and to brown after one week, indicating that rapid nucleation and sequent aggregation took place. Different experiments were also performed to explore the formation mechanism of the dendritic silver nanostructures.

As for experimental condition 2 (sample 2), the amount of 2 mM PA solution was decreased to 2 mL with other conditions unchanged.

As for experimental condition 3 (sample 3), the concentration of silver nitrate was increased to 7.4 mM with no change in other conditions.

Characterization. The samples for the TEM examination were prepared by adding a drop of aqueous solution onto a carbon-coated copper grid, then after one minute removing any excess solution by a filter paper, and finally allowing the samples to dry in air at room temperature. The samples for the XRD characterization were prepared on glass substrates by similar methods. A similar method was also used to prepare the samples for SERS. After drying the samples, a drop of 100 nM rhodamine 6G (R6G) was added to the samples for 40 min, and then they were dried by nitrogen gas. The TEM images were obtained on a TECNAI $F2OG_2$ TWIN transmission electron microscopy operating at 200 kV. The grid was inserted into a beryllium TEM specimen holder for EDS analysis; TEM images and analytical data were further processed by Digital Micrograph 3.7.0 (Gatan software, Inc) and ES Vision 4.0 (Emispec system, Inc). Structures of the samples were characterized by using a high-resolution X-ray diffractometer (Rigaku, SLX-2000). Cu Kα radiation (wavelength, 1.5405 Å) was used as an incident X-ray source (50 kV, 300 mA). Raman spectra were obtained with a NRS-2100 model Raman spectrometer (JASCO) equipped with a nitrogen-cooled CCD detector by using a 514.5-nm excitation laser. Data acquisition time was 10 s with two accumulations.

Results and Discussion

The formation of the dendritic silver nanostructures is simply achieved by the reduction of excess $AgNO_3$ by $NaBH_4$ in the presence of PA molecules at room temperature. Figure 1a shows a TEM image of the sample obtained under experimental condition 1 (sample 1, see Experimental Methods section), clearly indicating that the sample possesses a delicate dendritic nanostructure. Different from previously reported ones,[9−12] it seems that these "leaves" of this dendritic nanostructure consist of many single tabular crystals instead of simple nanosphere aggregates, and these "leaves" more resemble those in natural trees (Figure S1, see Supporting Information). A HRTEM image of a "leaf" tip reveals clear lattice fringes with an interplane distance measured to be 2.50 Å, which corresponds to the 3 × {422} lattice spacing of a face-centered cubic (fcc) metal silver that can be built by 3 sets of 3 × {422} spacing (Figure 1b).[18] The forbidden {422} planes are often observed in metal nanostructures in the form of thin plates or films.[19] We note that these parallel lattice fringes are maintained with almost perfect crystal arrangement. A closer look at Figure 1b reveals an interesting feature, namely, the presence of dislocations in

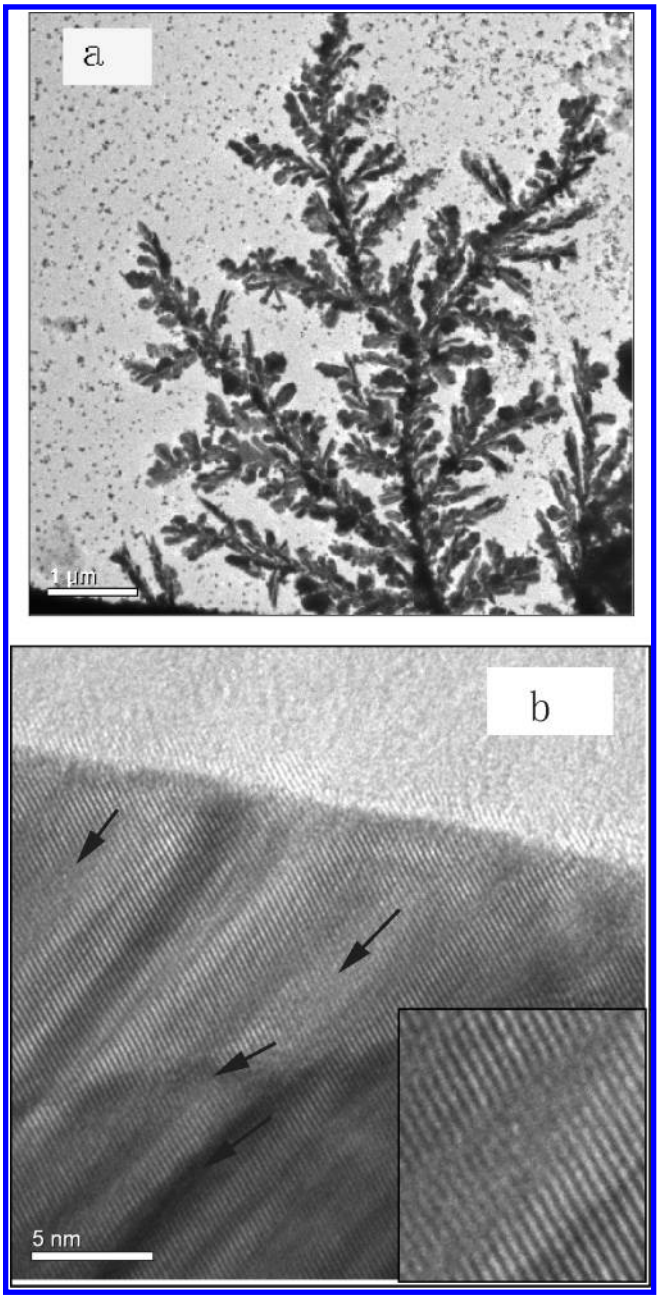

Figure 1. (a) A typical TEM and (b) a high-resolution TEM image of sample 1. Inset is the high-magnification image of the area highlighted by the above left arrow.

the "leaf" (highlighted by arrows). These dislocations can be easily observed from the high-magnification image (inset) although there exists clear lattice orientation in these boundary areas. The appearance of such dislocations is commonly considered to be a direct consequence of oriented attachment of particles, suggesting the occurrence of the initial particle−particle bonding.[15−17]

A high-magnification TEM image from the subbranch of the dendritic silver nanostructure and the selected area electron diffraction (SAED) patterns from the "leaf" part and the "trunk" part (highlighted by circles) are given in Figure 2a−c, respectively. It is noted that the "leaf" part and the "trunk" part show very similar SAED patterns characteristic of 6-fold rotational symmetry spots, implying that the basal planes of this subbranch are actually presented by {111} crystal planes.[19] The set consisting of six sharp spots with a spacing of 2.50 Å is due to 1/3 {422} reflections of fcc silver, very consistent with HRTEM

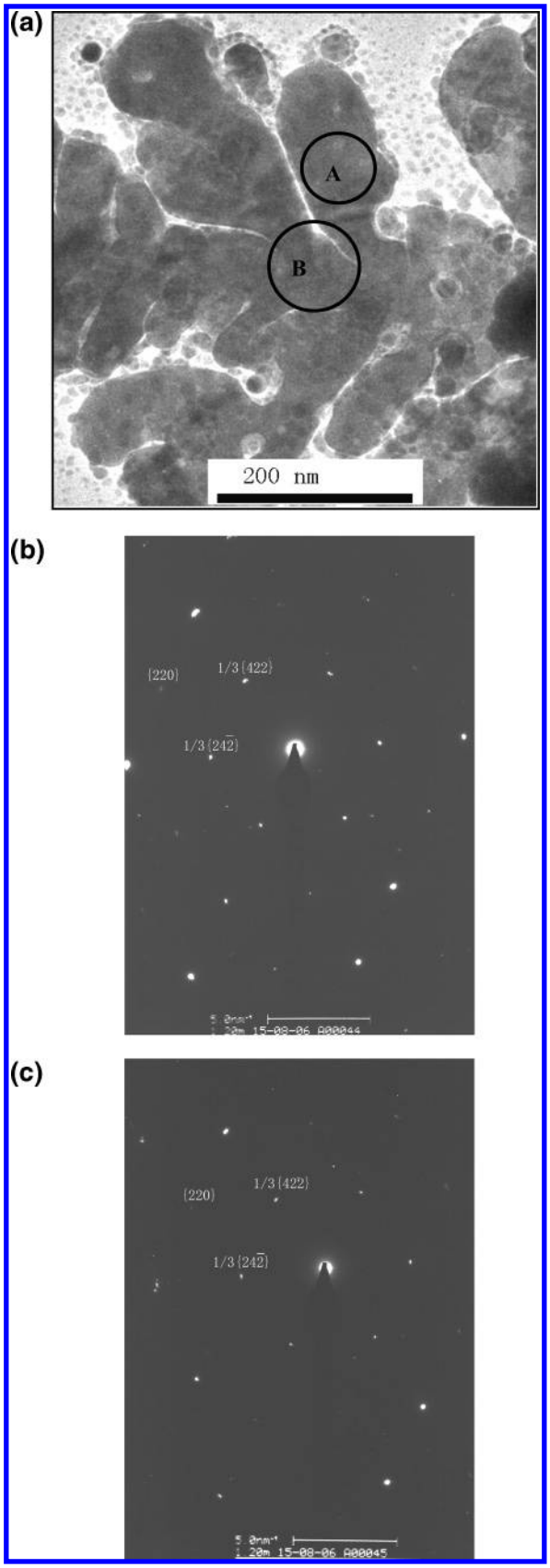

Figure 2. (a) A high-magnification TEM image of the subbranch of sample 1, and the corresponding SAED patterns of (b) the "leaf" part marked by circle A, and (c) the "trunk" part marked by circle B.

results.[18] Also, the weak spots corresponding to {220} reflections are observed. These results are significantly different from those previously found in the platelike gold, silver, and platinum nanostructures, in which the strongest spots are generally observed for the {220} reflections with weak spots of 1/3 {422} reflections.[19] Evident from SAED patterns, the (211) is the bonding plane for the "leaf" part, and thus preferential oriented growth of the "leaf" part is along the (211) direction. As for the "trunk" part, the (12$\bar{1}$) is the bonding plane, thus confirming that the formation of the "trunk" part originates from the preferential oriented growth along the (12$\bar{1}$) direction. Furthermore, the fact that the angle between the "leaf" part and the "trunk" part is measured to be about 60°, in accordance with the interplanar angle between the {211} planes and the {12$\bar{1}$} planes, provides strong evidence for our analysis based on SAED observation.

It is known that the reduction of $AgNO_3$ by $NaBH_4$ is an extremely rapid process due to the strong reducing ability of $NaBH_4$, which results in the formation of very small single-crystalline silver nanoparticles with a diameter of about 1.5−3 nm.[20] These small single-crystalline silver nanoparticles can walk freely in the solution, and Brownian motion-driven particle collisions will occur during this process. These collisions are especially effective if the particles make contact in a parallel lattice orientation, which leads to the reduction of total energy as a result of the elimination of the solid−liquid or solid−gas interface and an increase in entropy. Jiggling of small nanoparticles by Brownian motion may also allow adjacent particles to rotate to form a coherent particle−particle interface.[15] When the particles with the same crystalline orientation are approaching each other, there will be a driving force to form chemical bonds between atoms of opposing surfaces so as to achieve the full coordination.[15,16] However, these surfaces are not atomically flat. To achieve the coherent interface, an imperfect oriented attachment can also occur, which leads to the formation of dislocations between the neighboring particles.

TEM examination gives direct evidence in an early stage of the dendrite formation. Figure 3 presents TEM images of the sample collected after the reduction reaction of $AgNO_3$ by $NaBH_4$ in the presence of *p*-aminoazobenzene (PA) under experimental condition 1 for 5 min. At low magnification, nonuniform nanowires with a width of 1.5−15 nm are recognized besides a small amount of the spherical nanoparticles with a diameter of 1.5−8 nm. A more-detailed analysis can be made on the basis of the HRTEM images taken from a series of the nanowires in Figure 3b−d. HRTEM images show the clear lattice fringes that reveal that the nanowires originate from the oriented coalescence of small nanoparticles ranging from 1.5 to 8 nm. As for the silver nanoparticles with a diameter of 1.5−8 nm, their solubility in water is extremely low at room temperature. Hence, the Ostwald ripening process should be insignificant.[17] As a result, the oriented aggregation process becomes dominant in forming the nanowires, which can be seen by the bottlenecks between the adjacent particles in Figure 3b−d. However, these bottlenecks cannot be clearly distinguished in Figure 1b. It seems that the oriented attachment is the prerequisite for crystallite fusion, and subsequent coarsening should occur in this case.[5,15] Furthermore, imperfect oriented attachments are seen across some interfaces (highlighted by arrows). Such misorientation results in the introduction of dislocations in the nanowires. This is the reason the dislocations are recognized in Figure 1b.

High-angle annular dark field scanning TEM (HAADF/STEM) is a powerful tool for the characterization of nanostructured materials.[21,22] This technique provides high-resolution imaging capability with contrast due to difference in atomic number (*Z*), and it exhibits some advantage over bright-field

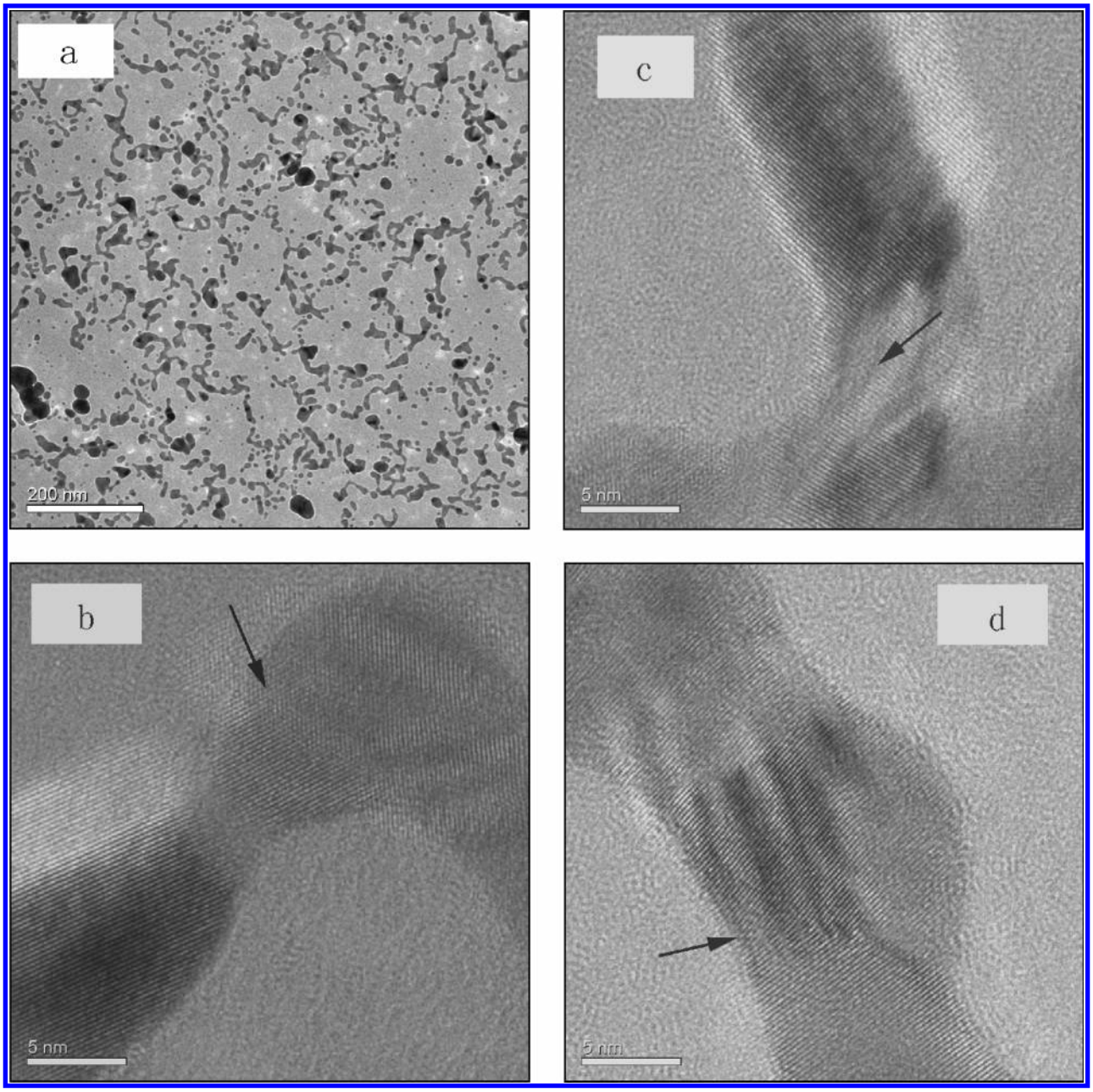

Figure 3. (a) A TEM image of the sample collected after the reduction reaction of $AgNO_3$ by $NaBH_4$ in the presence of *p*-aminoazobenzene (PA) for 5 min under experimental condition 1; (b−d) high-resolution TEM images of nanowires formed by an oriented attachment.

STEM. In HAADF/STEM images, the nanometer-scaled areas of increased average atomic number appear bright amidst a dark background because electrons scattered at small angles by lower average *Z* areas do not hit a HAADF detector.[21,22] Using HAADF/STEM, we imaged the as-prepared dendritic silver nanostructure. As shown in Figure S2 of Supporting Information, the dendritic nanostructure stands out clearly. The corresponding high-magnification image, shown in Figure 4a, clearly indicates that the "tree leaves", indeed, consist of many tabular crystals with a thickness range of 20−50 nm (highlighted by a rectangle). The surface of these tabular crystals are obviously not flat, and some "leaves" curl. Although the data are not shown here, we confirmed this by tilting the sample at 50 degree to the beam axis and observed the shape change. We further examined the chemical composition of the dendritic nanostructures by HAADF/STEM energy-dispersive X-ray spectroscopy (EDS). Strong peaks of the element Ag are observed in the EDS spectra of the selected "leaf" part and "trunk" part marked by a square, which further confirms that the as-prepared dendritic nanostructures consist of Ag (Figure 4b,c). Peaks of the element Cu are from the copper grid while that of the element C can be attributed to a carbon supporting film or PA molecules.

X-ray diffraction (XRD) was performed to further investigate the crystal structure of sample 1. Figure 5a presents the resulting XRD pattern. The peaks observed at $2\theta \sim 38.0°$, 44.0°, 64.2°, 77.1°, and 81.3° are assigned to the diffractions of (111), (200), (220), (311), and (222) planes of cubic metal silver, respectively (see the bulk reflexes, bottom of Figure 5). The cell parameter calculated from this XRD pattern is 4.08 Å, very consistent with the value reported in the literature (JCPDF No. 04-0783). Moreover, we find that the ratio between the maximum intensities of the (111) and the (200) diffraction lines is obviously larger than the value in JCPDF card (5 versus 2.5). Similar results are also observed for the ratio between the maximum intensities of the (111) and other diffraction lines. These results reveal that as for sample 1, the (111) planes tend

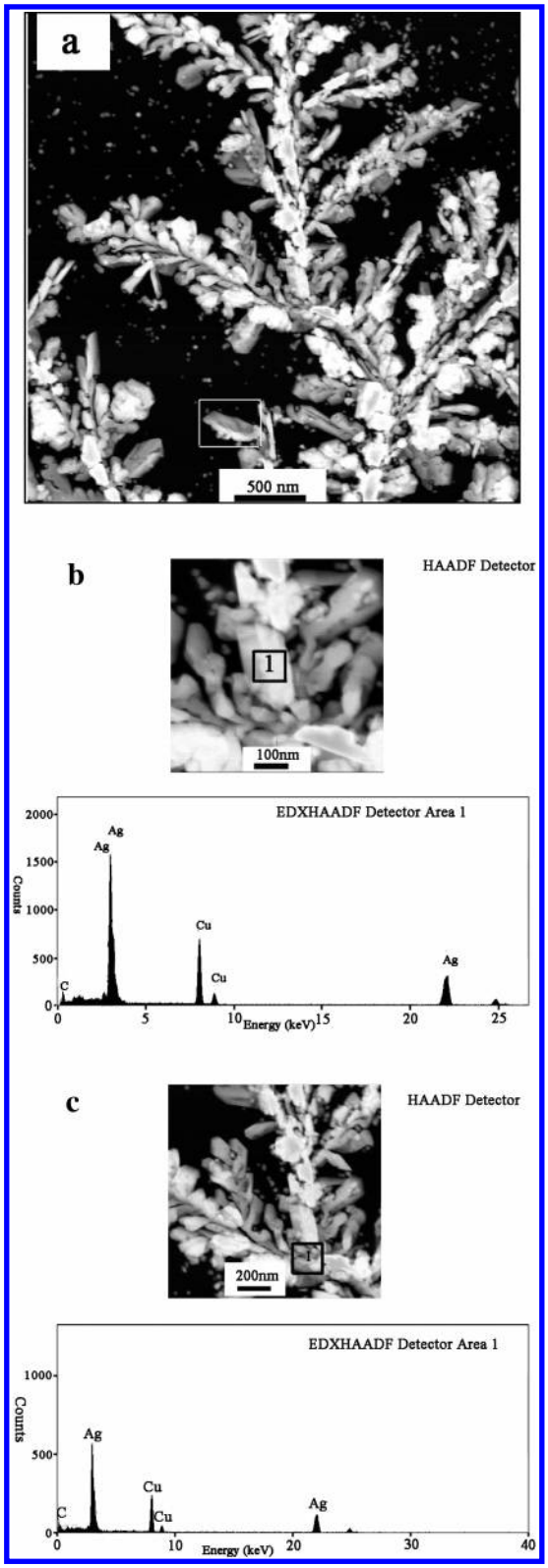

Figure 4. (a) A HAADF-STEM image of sample 1. HAADF/STEM/EDS spectra of (b) the selected "leaf" part, and (c) the selected "trunk" part in sample 1.

to be preferentially oriented parallel to the surface of the supporting substrate, thus giving a significantly high (111) reflection intensity, which also further confirms the above SAED results.[19]

To understand more about the formation mechanism of the dendritic silver nanostructures, we also performed different experiments. In the absence of the PA molecules, only spherical

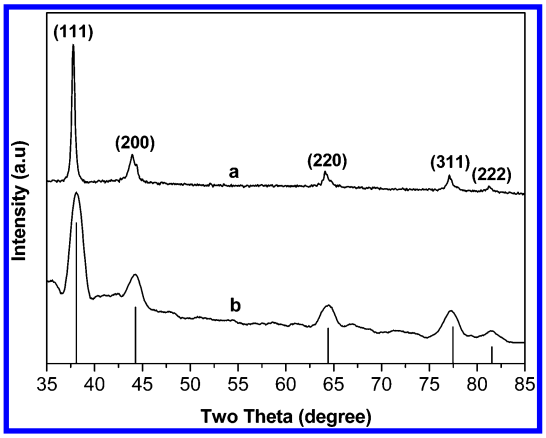

Figure 5. XRD patterns of (a) sample 1, and (b) sample 3.

silver particles were obtained. When the PA concentration was reduced to 40% of that used in experiment condition 1, similar dendritic silver nanostructures were formed. However, the size of "tree leaves" is obviously larger than that formed under experimental condition 1 (sample 2, Figure 6a). In contrast, when the PA concentration was increased, so that the final molar ratio of PA to the silver precursor was close to 1, no dendritic silver nanostructures were found. Doubling the silver precursor concentration over that used in experimental condition 1 results in the formation of very different dendritic silver nanostructures (sample 3, Figure 6b). It can be seen from a high-magnification TEM image that such nanostructures consist mainly of many nanocrystals (20−60 nm in length, Figure S3 of Supporting Information). HRTEM images show that they are single-crystalline. It is worth noting that these silver single crystals do not aggregate randomly, but attach to one another in an oriented way. As shown in Figure 6c,d, the crystalline lattice fringes are almost perfectly aligned between adjacent nanocrystals, and the corresponding FFT of the HRTEM images confirms that these nanoparticles assume the same crystallographic orientation. This experiment used a relatively large excess of $AgNO_3$, with a molar ratio of $AgNO_3$ to $NaBH_4$ of 3.7. This condition leads to fast nucleation and growth of silver nanoclusters, and may, therefore, reduce the time available for defects to form.[23,24] The corresponding XRD pattern of sample 3 shows the fcc structure of metal silver (Figure 5b).

We confirmed the above analysis using TEM investigations in an early stage of dendrite growth. Figure S4 (Supporting Information) shows a typical TEM image of the sample obtained after growing for 5 min. In contrast with Figure 3, large nanoparticles with a diameter of about 15−35 nm are seen adjacent to small nanoparticles with an average diameter of about 6 nm. HRTEM images reveal that they are single-crystalline. The above results imply that $AgNO_3$ should be employed in excess to maintain high chemical potential and, consequently, to produce perfect single-crystallites silver nanostructures.[22,23] These single-crystalline silver nanoparticles subsequently aggregate through the oriented attachment mechanism noted above. In the past studies on the solution-phase methods, the oriented attachment was generally observed between the adjacent smaller nanocrystals (typically below 10 nm), and relatively high temperature was required.[2,5,15−17] Recently, the oriented attachment was also found to occur between primary particles with a large size at relatively high temperature.[25−27] For example, Zeng et al. reported that hollow CuO microspheres could be built from the crystal strips with a thickness of 20−30 nm in the oriented attachment way at 180 °C.[25] A nonhydrolytic sol−gel process was demonstrated by

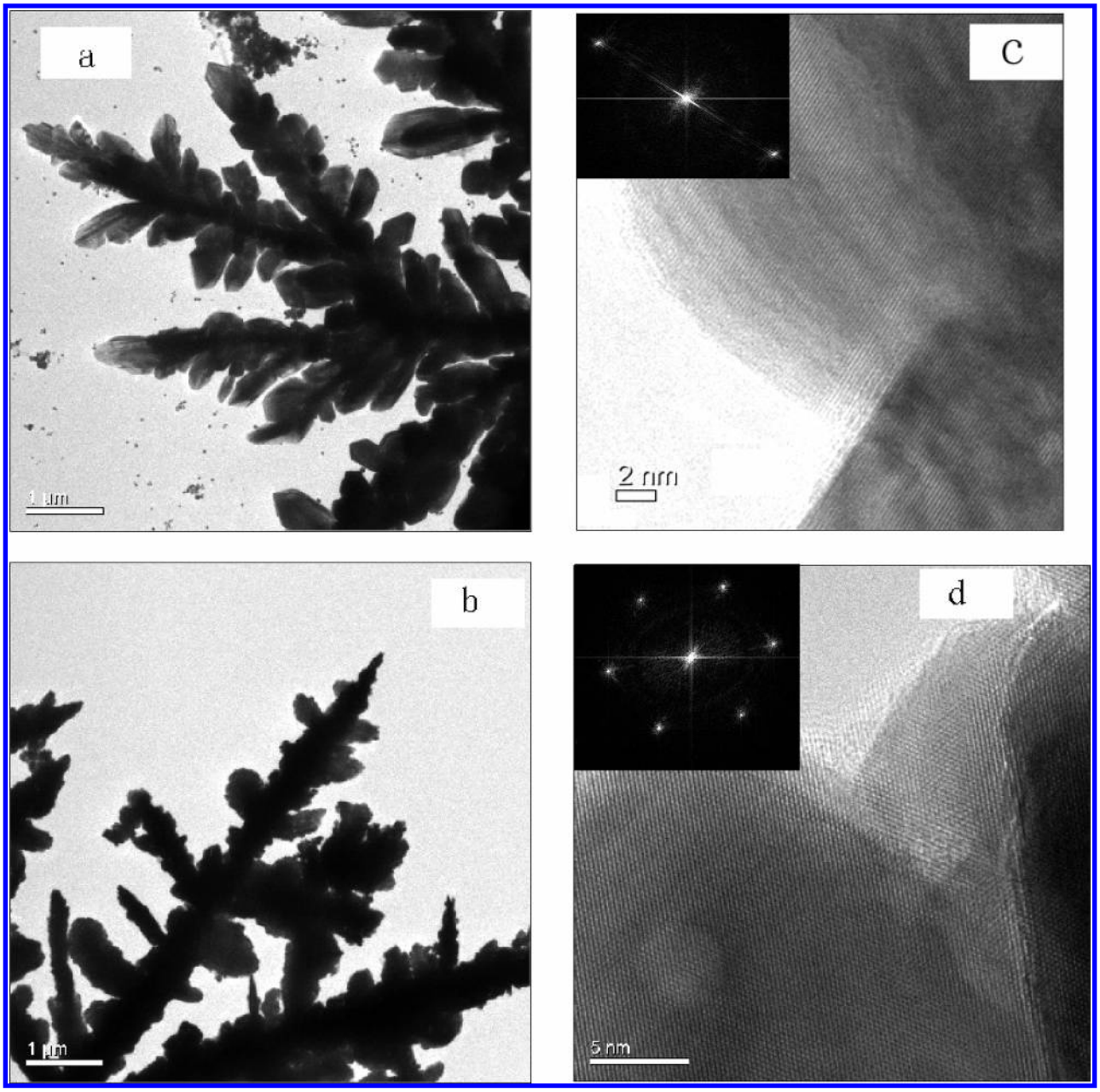

Figure 6. (a) A TEM image of sample 2. (b) TEM and (c,d) HRTEM images and corresponding FFT (inset) in different parts of sample 3.

Zitoun et al. to prepare single-crystal MnO multipods through the oriented attachment of the particles with sizes of 40−50 nm at 320 °C.[26] Wang et al. found that the oriented coalescence of $PbMoO_4$ particles with sizes of 30−60 nm could lead to the formation of the dendritic crystals at 160 °C, while the oriented coalescence of LaF_3 nanodisks with sizes of 20−50 nm enabled the preparation of the cylinder crystals at 160 °C.[27] These examples show that the nanostructures with complex shape, which are expected to exhibit novel properties, can be constructed through the oriented attachment of the large particles, thus providing new possibilities for the design of novel nanomaterials based on the oriented coalescence of large particles. In the present case, our observation of the oriented attachment of large silver particles in a system not subject to heat treatment (at room temperature) implies that this oriented attachment-based growth mechanism presents a very low activation energy. This is the first report that the oriented attachment at room temperature can occur between perfect silver nanocrystals with a relatively large crystal size. We believe that this finding is important for further understanding of the oriented attachment mechanism and, hence, the use of the preformed large metal nanoparticles as precursors in oriented attachment for building new and interesting artificial materials at room temperature.

The dendritic silver nanostructures may serve as excellent SERS substrates for investigating PA molecules adsorbed on their surfaces, which can be helpful for further understanding the role of the PA molecules during the crystal growth. For a comparison, a Raman spectrum of 2 mM PA molecules in an ethanol solution is presented in Figure 7A(a). This weak Raman peak from the PA molecules is in good agreement with its Raman data reported previously.[28] Figure 7A(b) and Figure 7B(a) depict SERS spectra of the PA molecules obtained from sample 1 and sample 3, respectively. It is clear that both sample 1 and sample 3 exhibit excellent enhancement efficiency with the 514-nm excitation. Although the concentration of the PA molecules under experimental condition 1 is the same as that under experimental condition 3, the intensity of the SERS signal

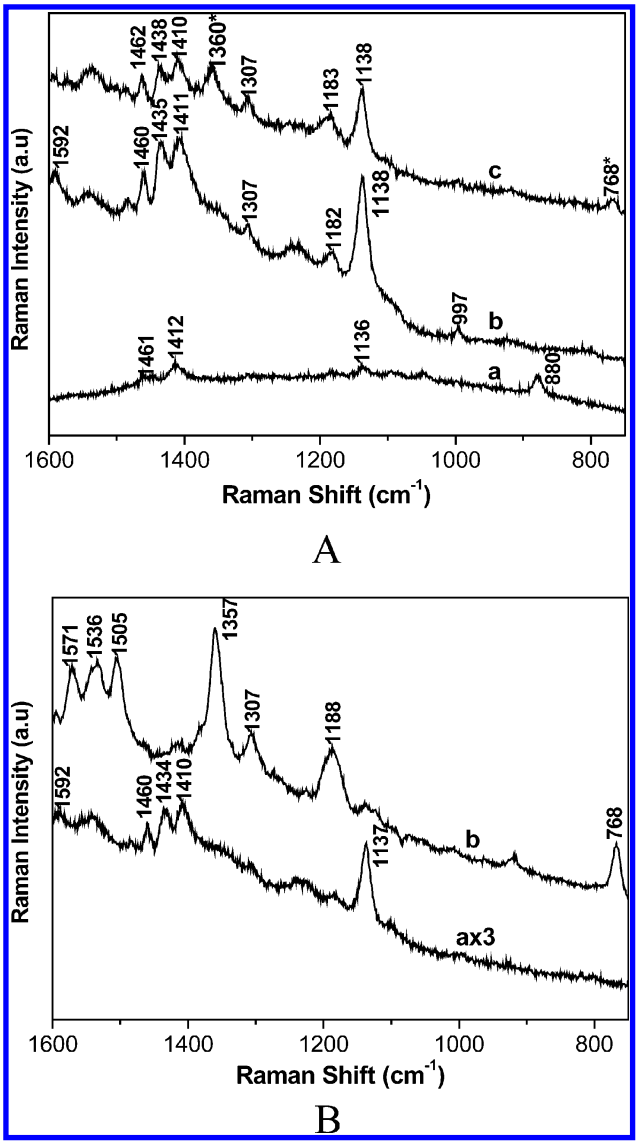

Figure 7. (A) (a) A Raman spectrum of PA molecules in an ethanol solution, and SERS spectra of (b) PA molecules, and (c) mixture of R6G and PA molecules on the surface of sample 1. (B) SERS spectra of (a) PA molecules and (b) R6G molecules on the surface of sample 3. Data acquisition time was 10 s with two accumulations. An asterisk in Figure 7A(c) corresponds to the peak from R6G molecules. The intensities of the spectra in Figure 7B(a) are multiplied by a factor of 3 for the purpose of comparison.

of the PA molecules from sample 1 is obviously stronger than that from sample 3. This may result from the difference in their morphologies and nanostructures.[29] To investigate the details of the PA molecules on the surfaces of the samples, we used 100 nM rhodamine 6G (R6G) to replace the PA molecules. Figure 7A(c) and Figure 7B(b) show the resultant SERS spectra obtained from sample 1 and sample 3, respectively. As observed from Figure 7A(c), only a small number of the PA molecules are replaced by R6G molecules, evidenced by the presence of the peaks at 1360 and 768 cm^{-1} characteristic of the R6G molecule, and the intensity of the SERS signal from the PA molecules obviously decreases after the replacement. In contrast, no characteristic peaks of the PA molecules are seen in the case of sample 3, suggesting that almost all PA molecules are replaced by R6G (Figure 7B(b)). As for sample 2, we obtained results similar to those of sample 1. The above SERS analysis clearly shows that the PA molecules are weakly adsorbed on the surfaces of the samples, and it is possible to replace them by the low-concentration R6G molecules.

On the basis of the above discussion, we suggest that the dendritic silver nanostructures are formed as follows. According to previous reports,[12,30−31] dendritic structures are obtained only when the anisotropy predominates over random noise during the growth process. In our present experimental system, only a little noise is introduced into the growth system. The anisotropy, which is essential for the formation of the dendritic nanostructures, results from the interactions between the particles and background, or the particles themselves. As mentioned above, the constituent nanocrystals in sample 1, sample 2, and sample 3 intrinsically contain a strong crystalline anisotropy. Therefore, the coalescence of these silver nanocrystals occurs mainly along the preferred direction such as the (211) and the $(12\bar{1})$ directions, and it leads to formation of the dendritic silver nanostructures. One important question remains here, that is why the morphologies of sample 1 and sample 2 are significantly different from that of sample 3. The above experimental results indicate that the concentrations of the PA molecules and the $AgNO_3$ have important effects on the formation of the dendritic silver nanostructures in our systems. The only difference between experimental condition 1 and experimental condition 2 lies in the concentration of the PA molecules. The PA molecules adsorbed on the surfaces of small silver nanoclusters can lower the opportunity for different collisions between them,[32] which is evidenced by our observation that the color change under experimental condition 1 is much slower than that under experimental condition 2. Furthermore, because the PA molecules, as evidenced by the above SERS experiment, adsorb weakly on the surfaces of small silver nanoclusters, it is possible for them to desorb from the surfaces, and the effective collisions between small nanoclusters can occur in the oriented attachment model. The decrease in the concentration of the PA molecules from sample 1 to sample 2 increases such collision chances, and thus the size of "leaves" in sample 2 grows larger than that in sample 1. In comparison, the concentration of the PA molecules under experimental condition 3 is equal to that under experimental condition 1, but the molar ratio of $AgNO_3$ to $NaBH_4$ increases twice as high as that under experimental conditions 1 and 2. As stated above, high chemical potential results in the fast formation of relatively large single-crystalline silver nanostructures, and these nanocrystals aggregate into the dendritic structures by the oriented attachment process. Moreover, selective adsorption of PA molecules on the different crystal planes of the silver nanoparticles may also play an important role in controlling the morphology of the dendritic silver nanostructures.[1d,19]

Conclusion

In summary, we have demonstrated the distinct types of hierarchical dendritic silver nanostructures. An oriented attachment-based aggregation model has been proposed to rationalize the formation of such nanostructures. Importantly, it is found that an oriented attachment process at room temperature also occurs between relatively large single-crystalline silver particles with a diameter of 20−60 nm, which may provide new possibilities for design of novel metal nanostructures based on the oriented attachment of large nanoparticles at room temperature. Due to their unique dendritic supramolecular nanostructures, these materials exhibit excellent SERS enhancement ability, thus providing an efficient method for investigating the role of organic molecules in directing the formation of the silver dendrites.

Acknowledgment. We thank Dr. He Huang for valuable discussion. This work was partially supported by "Open Research Center" project for private universities: matching fund subsidy from MEXT (Ministry of Education, Culture, Sports, Science and Technology), 2001-2008.

Supporting Information Available: Additional TEM and HAADF data. This material is available free of charge via the Internet at http://pubs.acs.org.

References and Notes

(1) (a) Zhang, J. Z.; Wang, Z. L.; Liu, J.; Cheng, S. W.; Liu, G. Y. In *Self-Assembled Nanostructures*; Kluwer Academic Publisher: New York, 2002. (b) Burda, C.; Chen, X. B.; Narayanan, R.; El-Sayed, M. A. *Chem. Rev.* **2005**, *105*, 1025. (c) Schmid, G. In *Nanoparticles from Theory to Application*; Wiley-VCH: Weinheim, Germany, 2003. (d) Murphy, C. J.; Sau, T. K.; Gole, A. M.; Orendorff, C. J.; Gao, J. X.; Gou, L. F.; Hunyadi, S. E.; Li, T. *J. Phys. Chem. B* **2005**, *109*, 13857.

(2) Pacholski, C.; Kornowski, A.; Weller, H. *Angew. Chem., Int. Ed.* **2002**, *41*, 1188.

(3) Peng, X. G.; Manna, L.; Yang, W. D.; Wichham, J.; Scher, E.; Kadavanich, A.; Alivisatos, A. P. *Nature (London)* **2000**, *404*, 59.

(4) (a) Lin, S.; Li, M.; Dujardin, E.; Girard. C.; Mann, S. *Adv. Mater.* **2005**, *17*, 2553. (b) Tang, Z.; Kotov, N. A.; Giersig, M. *Science* **2002**, *297*, 237.

(5) Giersig, M.; Pastorza-Santos, I.; Liz-Marzán, L. M. *J. Mater. Chem.* **2004**, *14*, 607.

(6) Cho, K.; Talapin, D. V.; Gaschler, W.; Murray, C. B. *J. Am. Chem. Soc.* **2005**, *127*, 7140.

(7) Yu, S. H.; Cölfen, H.; Antonietti, M. *Adv. Mater.* **2003**, *15*, 133.

(8) Lu, L. H.; Capek, R.; Kornowski, A.; Gaponik, N.; Eychmüller, A. *Angew. Chem., Int. Ed.* **2005**, *44*, 5997.

(9) (a) Selvan, S. T.; Hayakawa, T.; Nogami, M.; Möller, M. *J. Phys. Chem. B* **1999**, *103*, 7441. (b) Cao, M. H.; Liu, T. F.; Gao, S.; Sun, G.; Wu, X. L.; Hu, C. W.; Wang, Z. L. *Angew. Chem., Int. Ed.* **2005**, *44*, 4197.

(10) Peng, Q.; Dong, Y. J.; Deng, Z. X.; Li, Y. D. *Inorg. Chem.* **2002**, *41*, 5249.

(11) Parfenov, A.; Gryczynski, I.; Malicka, J.; Geddes, C. D.; Lakowicz, J. R. *J. Phys. Chem. B* **2003**, *107*, 8829.

(12) (a) Nittmann, J.; Stanley, H. E. *Nature (London)* **1986**, *321*, 663. (b) Sander, L. M. *Nature* **1986**, *322*, 789.

(13) Penn, R. L.; Oskam, G.; Strathmann, T. J.; Searson, P. C.; Stone, A. T.; Veblen, D. R. *J. Phys. Chem. B* **2001**, *105*, 2177.

(14) Wong, E. M.; Bonevich, J. E.; Searson, P. C. *J. Phys. Chem. B* **1998**, *102*, 7770.

(15) Banfield, J. F.; Welch, S. A.; Zhang, H. Z.; Ebert, T. T.; Penn, R. L. *Science* **2000**, *289*, 751.

(16) Penn, R. L.; Banfield, J. F. *Science* **1998**, *281*, 969.

(17) Ribeiro, C.; Lee, E. J.; Giraldi, T. R.; Longo, E.; Varela, J. A.; Leite, E. R. *J. Phys. Chem. B* **2004**, *108*, 15612.

(18) (a) Jin, R. C.; Cao, Y. W.; Mirkin, C. A.; Kelly, K. L.; Schatz, G. C.; Zheng, J. G. *Science* **2001**, *294*, 1901. (b) Jin, R. C.; Cao, Y. W.; Hao, E. C.; Métraux, G. S.; Schatz, G. C.; Mirkin, C. A. *Nature (London)* **2003**, *425*, 487.

(19) (a) Chen, S. H.; Carroll, D. L. *Nano Lett.* **2002**, *2*, 1003. (b) Hao, E. C.; Kelly, K. L.; Hupp, J. T.; Schatz, G. C. *J. Am. Chem. Soc.* **2002**, *124*, 15182. (c) Maillard, M.; Giorgio, S.; Pileni, M. P. *Adv. Mater.* **2002**, *14*, 1084. (d) Pastoriza-Santos, I.; Liz-Marzán, L. M. *Nano Lett.* **2002**, *2*, 903. (e) Xiong, Y.; McLellan, J. M.; Chen, J.; Yin, Y.; Li, Z. Y.; Xia, Y. *J. Am. Chem. Soc.* **2005**, *127*, 17118.

(20) (a) Van Hyning, D. L.; Zukoski, C. F. *Langmuir* **1998**, *14*, 7034. (b) Van Hyning, D. L.; Klemperer, W. G.; Zukoski, C. F. *Langmuir* **2001**, *17*, 3128.

(21) Weyland, M.; Midgley, P. A.; Thomas, J. M. *J. Phys. Chem. B* **2001**, *105*, 7882.

(22) Benetatos, N. M.; Smith, B. W.; Heiney, P. A.; Winey, K. L. *Macromolecules* **2005**, *38*, 9251.

(23) Peng, Z. A.; Peng, X. G. *J. Am. Chem. Soc.* **2002**, *124*, 3343.

(24) Wiley, B.; Sun, Y. G.; Mayers, B.; Xia, Y. N. *Chem.—Eur. J.* **2005**, *11*, 454.

(25) Liu, B.; Zeng, H. C. *J. Am. Chem. Soc.* **2004**, *126*, 8124.

(26) Zitoun, D.; Pinna, N.; Frolet, N.; Belin, C. *J. Am. Chem. Soc.* **2005**, *125*, 15034.

(27) (a) Cheng, Y.; Wang, Y. S.; Chen, D. Q.; Bao, F. *J. Phys. Chem. B* **2005**, *109*, 794. (b) Cheng, Y.; Wang, Y. S.; Zheng, Y. H.; Qin, Y. *J. Phys. Chem. B* **2005**, *109*, 11548.

(28) Machida, K.; Kim, B.; Saito, Y.; Igarashi, K.; Uno, T. *Bull. Chem. Soc. Jpn.* **1974**, *47*, 78.

(29) Kneipp, K.; Kneipp, H.; Itzkan, I.; Dasari, R. R.; Feld, M. S. *Chem. Rev.* **1999**, *99*, 2957.

(30) Ben-Jacob, E.; Godbey, R.; Goldenfeld, N. D.; Koplik, J.; Levine, H.; Mueller, T.; Sander, L. M. *Phys. Rev. Lett.* **1985**, *55*, 1315.

(31) Brune, H.; Romainczyk, C.; Röder, H.; Kern, K. *Nature (London)* **1994**, *369*, 469.

(32) Zhang, Z. P.; Sun, H. P.; Shao, X. Q.; Li, D. F.; Yu, H. D.; Han, M. Y. *Adv. Mater.* **2005**, *17*, 42.